Ground-Based Integrity Monitors for PPP Correction Services

Yu-Fang Lai, Juan Blanch, Todd Walter
Stanford University

BIOGRAPHY

Yu-Fang Lai is a Ph.D. candidate at Stanford GPS Lab. He received Bachelor's degree in Aero/Astro from National Cheng-Kung University in 2020, and Master's degree in Aero/Astro from Stanford in 2022.
Juan Blanch is a senior research engineer at Stanford University. He is a graduate of Ecole Polytechnique in France, he holds an M.S. degree in electrical engineering and a Ph.D. degree in aeronautics and astronautics from Stanford University.
Todd Walter is a Professor at Stanford University and the faculty of Stanford GPS Lab. He received his B.S. degree in physics from Rensselaer Polytechnic Institute and his Ph.D. degree in 1993 from Stanford University.

ABSTRACT

Integrity of Precise Point Positioning (PPP) is important for users with safety critical requirements, such as autonomous vehicles, that require sub-centimeter or centimeter level of positioning accuracy. It is therefore important for the provider of PPP network to guarantee the integrity of the broadcast corrections and the service itself is intact, and the network itself if capable of identifying and excluding the faulted satellite. For the integrity monitor system, we formulated an all-in-view centralized PPP filter dedicated to protecting the PPP user integrity in addition to the correction information necessary for the operation of PPP service. In this paper, we establish and simulate the operation of integrity monitor for PPP service. Specifically, we evaluate the satellite clock fault that happened on July 10th, 2023, and inject artificial satellite clock faults. The result shows we can correctly estimate the relative range errors in multi-fault scenarios with a constant bias, and the absolute user range errors after removing the bias. In summary, the all-in-view centralized filter can monitor all the satellites in-view to the receivers without applying solution separation on the satellites.

I. INTRODUCTION

Precise Point Positioning (PPP) is a positioning technique in GNSS that can achieve centimeter accuracy for static receivers, and sub-centimeter for receivers in kinematic scenarios. PPP carefully models the possible error sources of the pseudorange measurements and combine with the temporal and spatial relations of the receiver itself to estimate the receiver position and GNSS related estimations, such as tropospheric delay and ionospheric delay errors. In addition to this, PPP relies on external corrections to achieve centimeter positioning accuracy. These corrections are not contained in the broadcast navigation message but are generated and broadcast in different frequency bands, or from a third-party provider. Without the external corrections, the accuracy of the position estimation can only achieve 1$\sim$3 m. This is called Single Point Positioning (SPP). Therefore, the access and accuracy of the correction services for the PPP users is directly related to the integrity of the PPP users, which is crucial for any application with safety critical requirements. The integrity of the PPP users depends on the correction the PPP services provided.

For a single receiver, Advanced Receiver Autonomous Integrity Monitoring (ARAIM) can protect the integrity of the position solution (Blanch et al., 2015). ARAIM forms subset of snapshot position solutions, called solution separation, and each subset solution is computed from different number of measurement exclusions. The differences between the subset solutions contribute to the computation of the Protection Level (PL), which is a confidence bound to the position error and can be used to describe the level of integrity for the user position. Gunning et al. (2018) computes PL for the PPP by forming a subset of Extended Kalman Filters and position estimates in kinematic scenario. The challenge of ARAIM is the number of subset solutions grows in factorial as the number of measurements and exclusions increase. For receivers with multi-constellation or LEO-PNT availability the number of subset required may be impractical to compute. Blanch et al. (2024) addresses this issue by grouping the subset solutions with branch and bound algorithm that can greatly reduce the computations for the PL, at the cost of more conservative error bound.

However, the use of ARAIM inevitably creates extra computational cost to the user receivers. In our precious work (Lai et al., 2024), we proposed a PPP integrity monitor system using measurements from a network of ground receivers to monitor the possible satellite faults and the corresponding corrections. We monitor the potential ephemeris error and satellite clock bias error, which may be from either the satellites or the corrections. They are two of the most important sources of pseudorange error that are corrected by the PPP correction service. The monitor system uses a centralized EKF filter that can directly measures

the amount of ephemeris and satellite clock bias error in terms of pseudorange error at the user location. The PPP users only need to receive the pseudorange error information to ensure they are aware of the effect from the potential ephemeris faults and satellite clock faults, and the integrity of the users are protected. The weakness of the integrity monitor in our previous work stems from it can only monitor one satellite at a time, meaning it is vulnerable to the multi-fault scenarios where if more than 2 satellites are faulted at the same time, the monitor system would fail or misdetect.

In this paper, we consider multi-fault scenario. In Sec.III, we augment the number of satellites monitored by the centralized filter from single satellite to all the satellites in-view to the receivers. Additional constraints are applied to the filter to make the system observable and estimation meaningful. We used code phase and carrier phase measurements of GPS constellation collected from 15 different IGS (2024) receivers on July 10th, 2023, when GPS PRN-1 (SVN-63) experienced a -40 m step fault. We also injected 2 different artificial satellite clock faults along with the original step fault to evaluate the performance of the all-in-view centralized filter. It is shown in Sec.IV that the all-in-view centralized filter can estimate the correct relative user range errors of all the satellites at both single fault and multi-fault scenarios using single filter. The estimate of the user range error at the user location is offset by a constant bias due to the constraints. In Sec.V, we obtain the absolute range error estimate after identifying the faulted satellites and applying the bias correction. Finally, Sec.VI include Galileo constellation, in addition to GPS, into the filter to increase the confidence in rejecting faulted satellites.

II. IGS DATASET

The International GNSS Service, IGS (2024), has 514 GNSS receiver stations world-wide as of Feb. 10th 2024 and it provides free access to various GNSS products. The number of stations available may vary from days to days due to new stations being introduced, old stations retired, maintenance or events such as power outage.

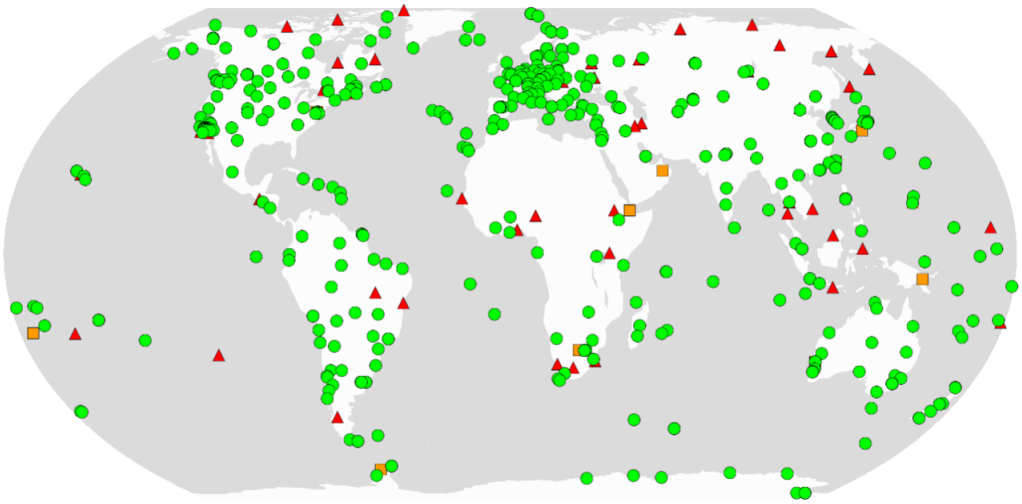

Figure 1: IGS Map and stations. IGS (2024)

In this paper, we used 30(s) interval GNSS measurements from IGS receivers and precise GNSS products, including precise ephemeris (.SP3 file), precise satellite clock bias (.CLK file), Differential Code Bias (.BIA file), Antenna Phase Center Offset (.ATX file) and the estimated receiver position as prior obtained from precise solution (.SNX file).

III. CENTRALIZED PPP FILTER

1. State Definition

This paper uses Extended-Kalman Filter (EKF) to realize PPP accuracy for the estimation of the GNSS related states. Consider the GNSS measurements are dual-frequency code and carrier phase pseudorange, we can define a standard receiver state for

single receiver as:

$$\overrightarrow{x_i} = \begin{bmatrix} x_i \\ y_i \\ z_i \\ v_{x,i} \\ v_{y,i} \\ v_{z,i} \\ b_i \\ \nabla b_i \\ \nabla \hat{T}_i \\ A_i^{(1)} \\ \vdots \\ A_i^{(k)} \end{bmatrix} \tag{1}$$

where $\overrightarrow{x_i}$ is the i^{th} receiver state. x_i, y_i, z_i are receiver position in Earth-Center-Earth-Fixed (ECEF) coordinate. $v_{x,i}, v_{y,i}, v_{z,i}$ are receiver velocity in ECEF coordinate. b_i is receiver clock bias. ∇b_i is receiver clock drift. $\nabla \hat{T}_i$ is tropospheric wet delay offset in zenith direction. $A_i^{(k)}$ is the floating ambiguities of k^{th} carrier phase measurement.

The ephemeris error and satellite clock bias error are estimated by the detection state, which is defined as:

$$\overrightarrow{D_j} = \begin{bmatrix} \zeta_j \\ \Delta \overrightarrow{\gamma}_j \end{bmatrix} \tag{2}$$

where $\overrightarrow{D_j}$ is the detection state of the j^{th} satellite. In other words, $\overrightarrow{D_j}$ estimates the ephemeris error and satellite clock bias error of the j^{th} satellite. ζ_j is the satellite clock bias error. This is a geometric-free error, which will cause the same amount of pseudorange errors across the receivers located at different places. $\Delta \overrightarrow{\gamma}_j$ is a 3×1 vector estimating the satellite translational error in ECEF coordinate:

$$\Delta \overrightarrow{\gamma}_j = \begin{bmatrix} \Delta x_j \\ \Delta y_j \\ \Delta z_j \end{bmatrix} \tag{3}$$

This is a geometric error. Receivers located at different places will experience different amount of pseudorange errors due to varying relative direction relative to the satellite.

Finally, for a centralized PPP filter monitoring all the satellites in-view to all the receivers, we can define its state as:

$$\overrightarrow{x} = \begin{bmatrix} \overrightarrow{x_1} \\ \overrightarrow{x_2} \\ \vdots \\ \overrightarrow{x_i} \\ \vdots \\ \overrightarrow{x_n} \\ \overrightarrow{D_1} \\ \overrightarrow{D_2} \\ \vdots \\ \overrightarrow{D_j} \\ \vdots \\ \overrightarrow{D_m} \end{bmatrix} \tag{4}$$

where $\overrightarrow{x}$ is the state for the centralized PPP filter. $\overrightarrow{x}$ estimates n number of receiver states and m number of satellites. That is, there are n receivers in the monitor system, and m satellites in-view to the receiver network. In order for the estimation of

ephemeris error observable, there have to be at least 4 receivers in-view to each of the satellite, otherwise the satellites with under 4 receivers in-view have to be excluded.

2. Measurement Models

The measurement models of the centralized filter are dual-frequency Ionospheric Free (IF) models for code phase and carrier phase measurements.

$$\rho_{\text{IF}}^{(j)} = \| \overrightarrow{x}_s^{(j)} - \overrightarrow{x}_{rx} + \Delta \overrightarrow{\gamma}_j \| + \left(b - b_s^{(j)} \right) + m^{(j)} \nabla \hat{T} + R_m + \zeta_j + \epsilon^{(j)} \tag{5}$$

$$\phi_{\text{IF}}^{(j)} = \| \overrightarrow{x}_s^{(j)} - \overrightarrow{x}_{rx} + \Delta \overrightarrow{\gamma}_j \| + \left(b - b_s^{(j)} \right) + m^{(j)} \nabla \hat{T} + A^{(j)} + R_m + \zeta_j + \epsilon^{(j)} \tag{6}$$

where $\rho_{\text{IF}}^{(j)}$ is the code phase model of the j^{th} satellite, and $\phi_{\text{IF}}^{(j)}$ is the carrier phase. $\overrightarrow{x}_s^{(j)}$ is the satellite position (ephemeris). $\overrightarrow{x}_{rx}$ is the receiver position. $\Delta \overrightarrow{\gamma}_j$ is the ephemeris error estimate. b is the receiver clock bias and $b_s^{(j)}$ is the satellite clock bias. $m^{(j)}$ is the mapping function of the tropospheric delay, a scalar maps tropospheric delay from zenith to slant direction. $\nabla \hat{T}$ is the estimated tropospheric wet delay offset in zenith direction. ζ_j is the satellite clock bias error estimate. $A^{(j)}$ is the floating ambiguities. R_m is the modelled error sources for the centralized PPP filter, and $\epsilon^{(j)}$ is all the unmodelled effects. All terms are converted to meters. The error sources modelled in R_m include satellite antenna phase center offset, relativistic effects, solid earth tide modeling, ocean loading, modeled tropospheric delay, Sagnac Effect, phase wind up for carrier phase measurements and differential code bias.

3. Constraints

A number of constraints can be applied to the centralized filter to reduce convergence time and make the system observable.

a) Static Constraint

The GNSS receivers from IGS are stationary and the true position of the receivers had already been pre-computed. As a result, the receiver position estimate, x_i, y_i, z_i, can be constrained to be constant values x_t, y_t, z_t. The velocity, $v_{x,i}, v_{y,i}, v_{z,i}$, can then be constrained to 0. The constraints are simply:

$$x_i = x_t \tag{7}$$

$$y_i = y_t \tag{8}$$

$$z_i = z_t \tag{9}$$

$$v_{x,i} = 0 \tag{10}$$

$$v_{y,i} = 0 \tag{11}$$

$$v_{z,i} = 0 \tag{12}$$

b) Zero Mean Constraint

The centralized filter consists of detection states for all the satellites measurement available to the receivers. This results in the system is unable to distinguish the estimation of receiver clock bias and satellite clock bias. That is, the system is unobservable from GNSS measurements. An additional constraint needs to be enforced to make the estimate of the detection state observable. A reasonable choice of constraints is constraining the mean of all the projected user range errors to be zero at the receiver positions.

The i^{th} receiver position $\overrightarrow{x}_{\text{i}}$.

The line-of-sight vector from $\overrightarrow{x}_{\text{i}}$ to the j^{th} satellite, $\overrightarrow{x}_j^s$, is a unit vector:

$$\overrightarrow{l}_{i,j} = \frac{\left(\overrightarrow{x}_j^s - \overrightarrow{x}_i \right)}{| \overrightarrow{x}_j^s - \overrightarrow{x}_i |}$$

The projected user range error from the j^{th} satellite at i^{th} position:

$$\beta_{i,j} = \zeta_j + \Delta \overrightarrow{\gamma}_j^{\top} \cdot \overrightarrow{l}_{i,j}$$

Therefore, the zero mean projected range error can be represented as:

$$\frac{\beta_{1,1} + \beta_{1,2} + ... + \beta_{n_{\text{rec}},n_{\text{sat}}}}{n_{\text{rec}} \cdot n_{\text{sat}}} = 0 \tag{13}$$

which can be simplified to:

$$\beta_{1,1} + \beta_{1,2} + ... + \beta_{n_{\text{rec}},n_{\text{sat}}} = 0 \tag{14}$$

or in a more compact form:

$$\sum_{i=1}^{n_{\text{rec}}} \sum_{j=1}^{n_{\text{sat}}} \beta_{i,j} = 0 \tag{15}$$

In short, the constraints for the centralized PPP filter are eqs. (7) to (12) and (15)

The choice of constraints is somewhat arbitrary. It can be any relation between the satellite clock bias error and ephemeris error with the receiver states. In the integrity monitor system, the essential product is the projected user rage error, and enforcing zero mean relations among the projected user range errors allows easier post-process and interpretation to the user range error estimate. This advantage is illustrated in the following sections.

IV. RELATIVE RANGE ERROR

July 10$^{\text{th}}$, 2023, GPS satellite PRN-1 (SVN-63) experienced a satellite clock fault, causing the user range error to offset by -40 m for around 20 minutes before it switched to non-standard code, and then marked unhealthy. The step fault lasted for around 12 hours before it was corrected. Due to this abnormal behavior and several faults and anomalies happened on Jan. 15$^{\text{th}}$ and Jan. 18$^{\text{th}}$ in the same year. SVN-63 was retired on Aug. 10$^{\text{th}}$ and SVN-44 was reactivated and operates under PRN-22 as the replacement to PRN-1(SVN-63).

In this section, we use GPS pseudorange measurements from 15 different receivers during the July 10 $^{\text{th}}$ fault to demonstrate the all-in-view centralized filter in actual satellite fault scenario. Additionally, we inject artificial satellite clock faults to other satellites to simulate the situations of multiple faults happen simultaneously.

There are 15 receivers from IGS network used in the paper, and their station code are GODN, HLFX, UNB3, NRC1, VALD, SCH2, ALBH, PIE1, NIST, SGPO, NLIB, MDO1, JPLM, BAMF and QUIN respectively.

The user range errors copmuted in the rest of the paper is projected to GODN station position to do comparison.

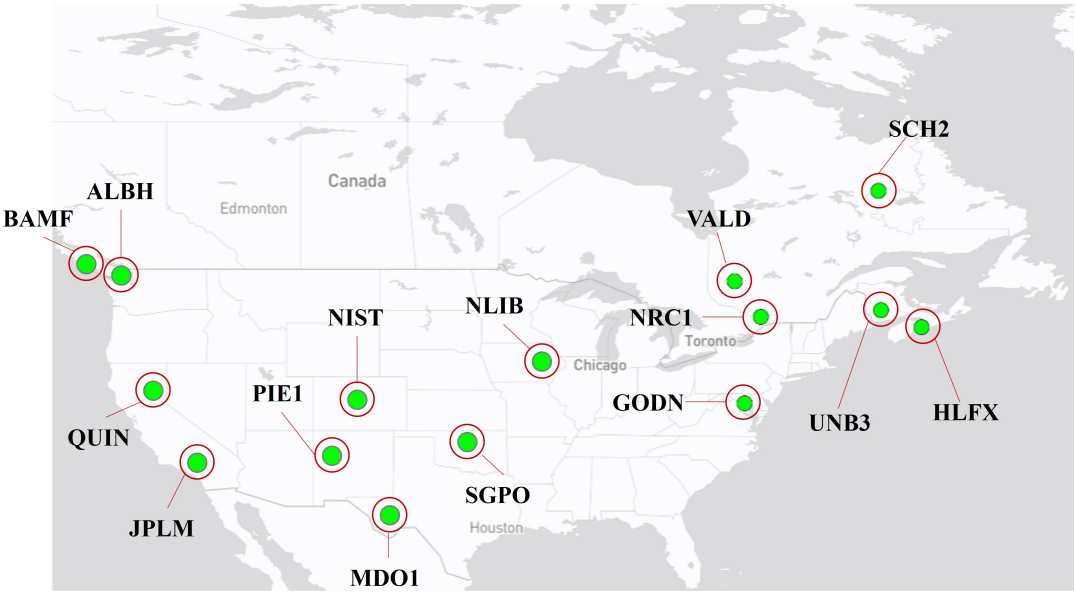

Figure 2: 15 IGS stations used.

1. Single Satellite Clock Fault

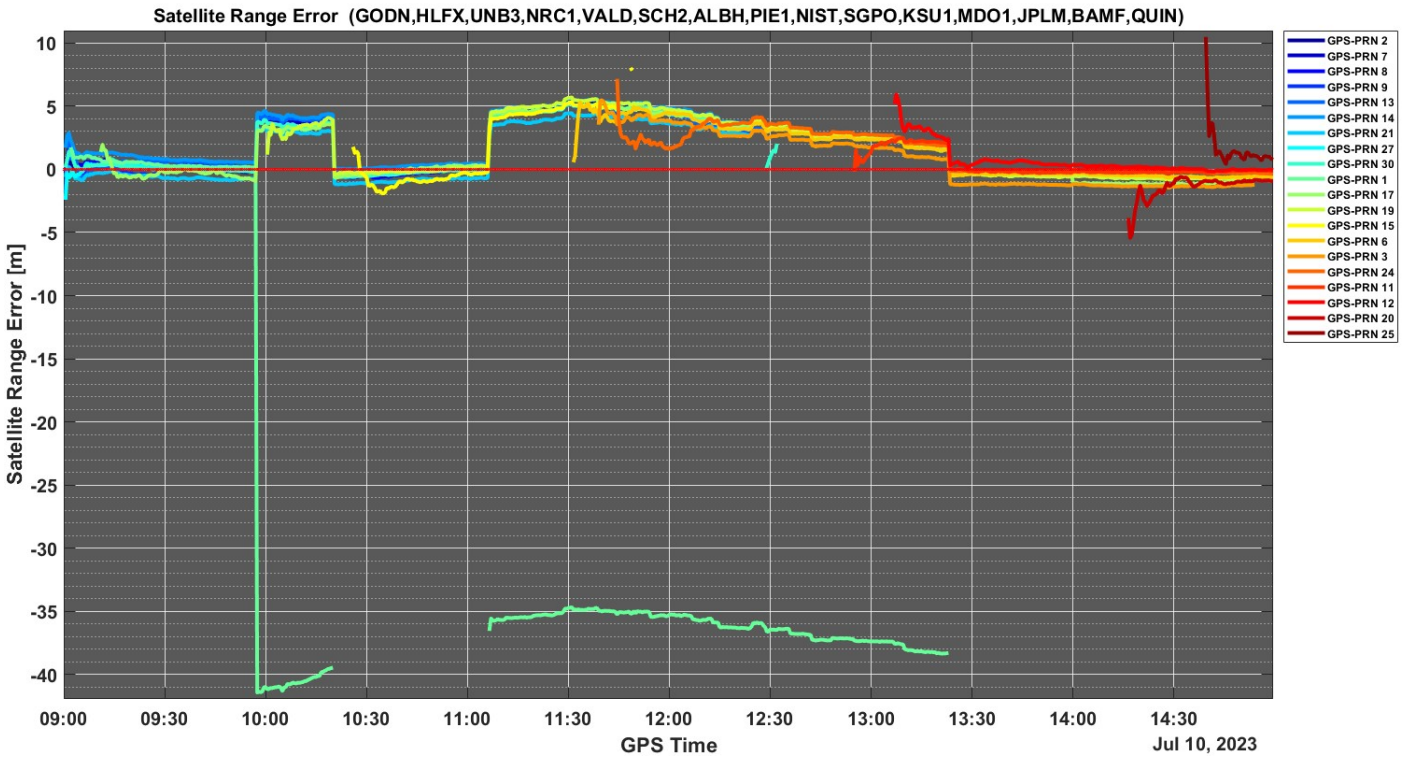

Figure 3: Single fault user range error estimate.

Fig.3 is the relative user range errors at the GODN receiver position for all the satellites that are in-view to receivers. We can see at 09:57:30, the user range error estimate of PRN-1 drops to around -36 m, and all the other user range error estimates raise to around 4 m. At 10:20:00, the PRN-1 signal switches to non-standard code so no sigal from PRN-1 is received. The PRN-1 is

switched back to standard code at 11:08:00 and marked unhealthy in the navigation message. The fault persists until PRN-1 is out-of-view from the receivers. The summation of the range error estimates is closed to zero at any point during the estimation. These are consistent with the constraints we have for the user range error estimates. It is apparent that the large displacement of the user range error estimate from PRN-1 is due to the -40 m clock fault, and the other user range error estimates are due to zero mean constraint we enforced.

Without knowing PRN-1 is at fault, we can still infer from the user range error estimates which satellite is most likely to be faulted. There are two possibilities for having user range error estimates behave as Fig.3. The first possibility is there is a large satellite fault happened on PRN-1 leads to the large user range error at the GODN receiver position. All the other satellites operate normally without faults. The second possibility is the entire GPS constellation is faulted except the PRN-1 behaves normally. This means at the onset of the fault, there are 9 satellite clock faults all having around 4 m user range error, and the zero mean constraint drives the user range error estimate of PRN-1 to -36 m. PRN-1 continues to behave normally and other satellites are still faulted even if there are new satellites in-view to the receivers. The first case is apparently more likely than the second case. Therefore, we can conclude that PRN-1 is most likely to be faulted, and all the other satellites are normal.

We can see when new satellites come in-view to the receiver network, there is convergent process for the user range error estimates before they stabilize to the nominal value. This is due to the convergence of ambiguities from the carrier phase measurement. To avoid confusion when interpreting estimation result, we only show the range error estimates with standard deviation less than 5 m in the rest of the paper. In other word, we are only interested in the estimate after convergence.

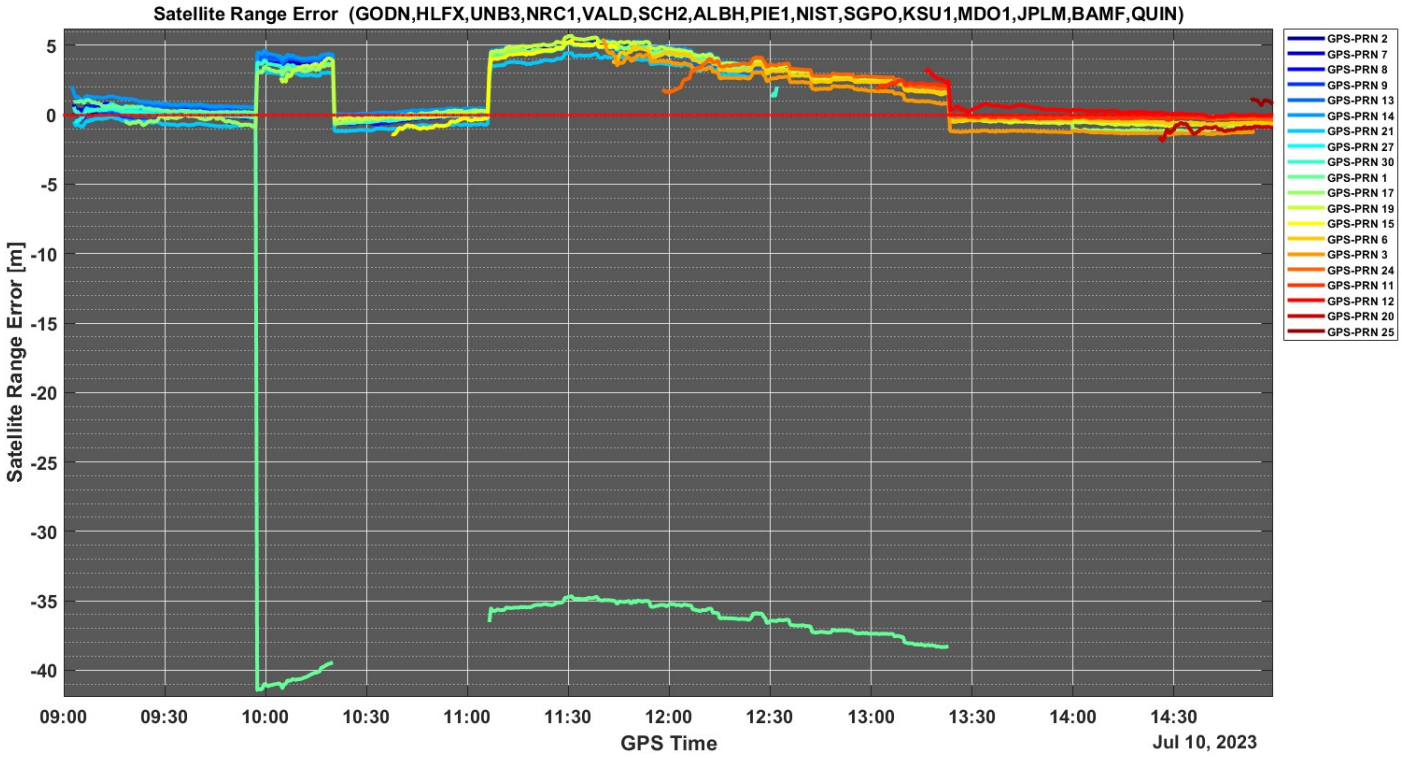

Figure 4: Single fault user range error estimate.

It is clear that there is a constant bias correction for all the user range error estimates. After identifying which group of satellites is normal, we can then compute the mean of the normal group as the bias, then subtract all the estimate of the user range errors such that the mean of the normal satellites is zero after adjustment, and the faulted satellites represent the user range error estimate of the satellite faults.

a) Multiple Satellite Faults

One additional artificial fault is injected to the pseudorange measurement to demonstrate the multi-fault scenario. The artificial fault is a ramp fault on PRN-19 with fault rate 0.01 m/s. It begins at 10:00:00 and ends at 12:00:00.

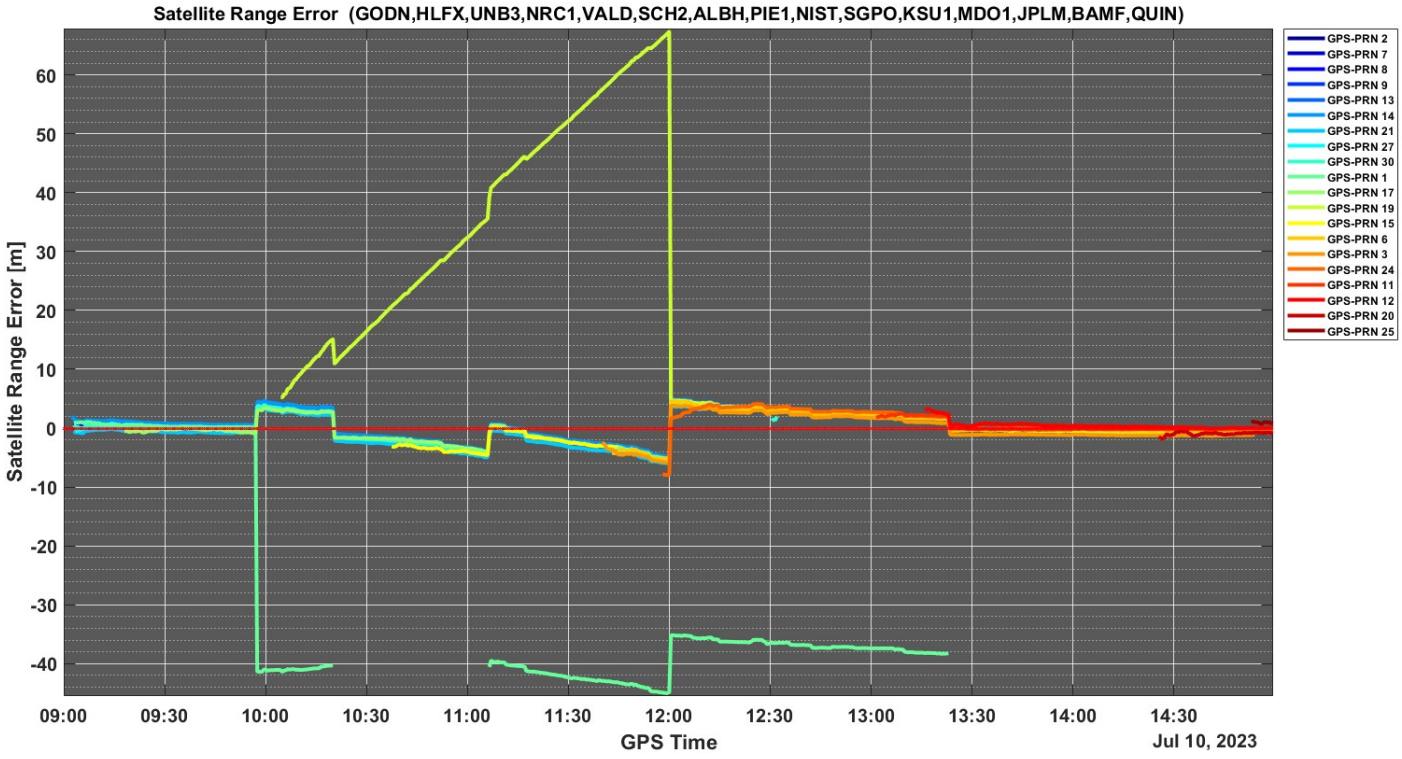

Figure 5: Multiple faults user range error estimate.

Fig.5 is the projected user range errors with 2 different faults happened at the same time. The user range error of PRN-1 drops at the onset of the -40 m satellite clock fault. At 10:00:00, PRN-19 increases as the ramp fault builds up in the pseudorange. After 12:00:00, we stop injecting fault to PRN-19, and the user range error estimates of this satellite immediately becomes part of the normal satellites. The user range error estimates of all the other satellites congregated are raised due to the zero-mean constraint. Since the sum of all the user range error estimates are zero, we can obtain the unbiased range error estimate by translating the mean of the normal satellites to zero.

V. FAULT IDENTIFICATION AND ABSOLUTE USER RANGE ERROR DETERMINATION

One strategy for identifying normal and faulted satellites would be finding the user range error bias of all the user range errors such that the likelihood is the most likely after applying such bias to all range error estimates. This strategy relies on assuming at least more than half of the satellites are in normal condition and the faulted satellites are simply the outliers. If more than half of the satellites in the constellation are faulted, the user range error bias would translate the mean of faulted satellites and results in misdetection. The probability of misdetection can be reduced with more satellites included into the centralized filter.

Given the assumption that half of the satellites in-view to the receiver network are normal. A simple way of finding outliers is choosing the median of the user range error as the base point, then normalize all the user range error estimates with their standard deviation. Any normalized user range error that is outside the threshold of standard normal distribution from the median base point is considered as outlier, which is the faulted satellite.

$$\beta_{med} = Median\left(\beta_j\right), i \in \{1, \ldots, n_{sat}\}$$
$$S_j = \frac{\beta_j}{\sigma_j}$$

where β_j is the projected user range error from the jth satellite, σ_j is the standard deviation of β_j, and S_j is the normalized user range error.

The outliers are determined by choosing S_j such that they are outside the pre-defined threshold of the standard normal distribution

with β_{med} as the mean. In this paper, a threshold of 5% is chosen.

$$j^{\text{th}} \text{ satellite} \begin{cases} \text{Faulted}, & \text{if } \|S_j - S_{med}\| > K \\ \text{Normal}, & \text{otherwise} \end{cases}$$

where K is 1.96 for 5% standard normal threshold.

After identifying the normal and faulted satellites, we translate the mean of the normal group satellites to zero, along with the faulted satellites, to obtain the absolute user range error. This step is justified that the user range errors of normal satellites should be zero mean distributed.

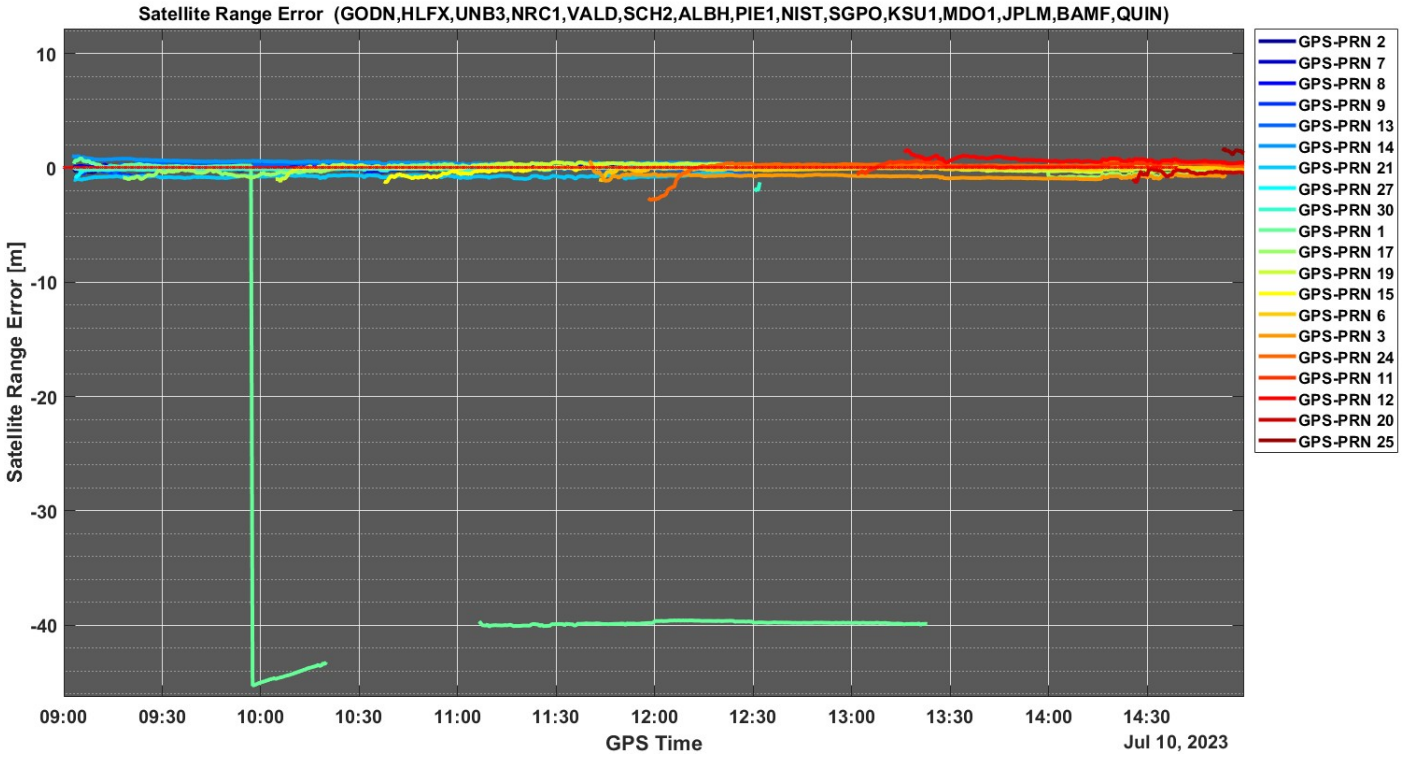

Figure 6: Single fault absolute user range error estimate.

Fig.6 is the absolute user range errors of Fig.4 after identifying the faulted satellites (PRN-1) and determining the absolute user rang errors. We can see PRN-1 has -40 m user rang error.

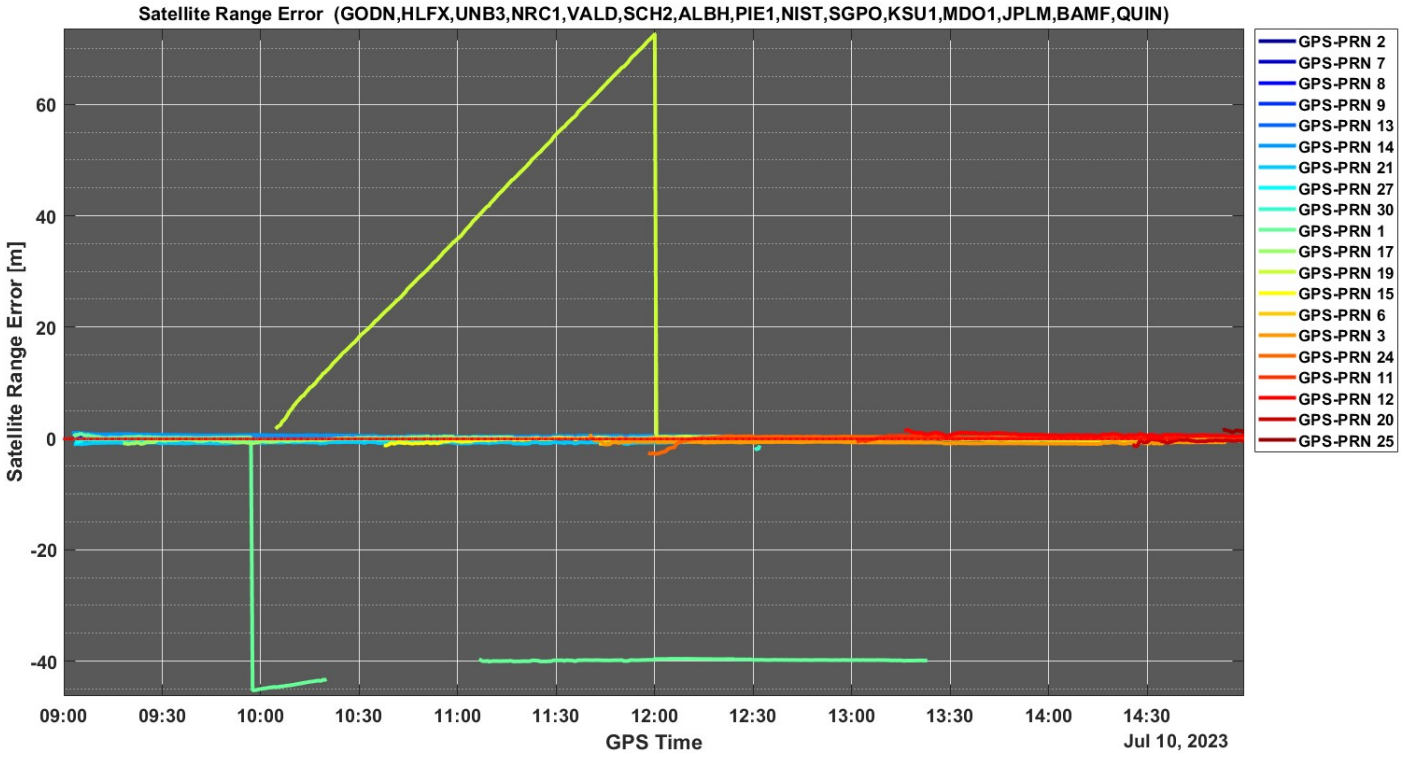

Figure 7: Multiple faults absolute user range error estimate.

Similarly, Fig.7 is the absolute user range errors of Fig.5.

The post-process to the user range errors described in this section allows integrity monitor system to detect multiple faulted satellites and estimate user range errors at the same time without applying solution separation on the satellites. There is only one filter, the centralized filter, used to monitor all the satellites in-view to the receiver network.

VI. MULTI-CONSTELLATION FAULT MONITORING

The important assumption we made when identifying faulted satellites from the relative user range error estimates is more than half of the satellites in-view are normal. The outlier exclusion cannot guarantee the outliers are faulted satellites if more than half of the satellites are faulted. While this situation is very unlikely to happen, we can still utilize this fact to reduce the probability of misdetection by including more satellites into the filter. As a result, it is beneficial to enable multi-constellation monitoring for the filter. In this section, we include satellites from Galileo constellation, in addition to GPS, with the same set of receiver network given the receivers receive signals from both GPS and Galileo constellation.

A necessary modification to the centralized filter is the use of measurement models. The standard approach for PPP with multi-constellation measurements is adding an additional receiver clock bias for the corresponding constellation. For instance, for a receiver receiving both GPS and Galileo signals, there are 2 receiver clock bias states, one for GPS and another one for Galileo. This approach becomes a problem for the centralized filter since the new receiver clock bias state for Galileo signals introduce an additional uncertainty to the system, which means the system is no longer observable and a second zero-mean constraint is required, which will effectively separate the user range error estimates of GPS and Galileo. In other words, adding additional receiver clock bias for Galileo is equivalent to having two centralized filters monitor GPS and Galileo satellites independently. Thus, we will not benefit from including another constellation.

To avoid introducing another uncertainty to the system, we relate the receiver clock bias of GPS and Galileo with an additional state, receiver dependent GPS-Galileo time offset, $\Delta\beta_{\text{GPS,GAL}}$.

$$\rho^{(j)}_{\text{IF,GPS}} = \| \overrightarrow{x}^{(j)}_s - \overrightarrow{x}_{rx} + \Delta\overrightarrow{\gamma}_j \| + \left(b_{\text{GPS}} - b^{(j)}_s \right) + m^{(j)} \nabla \hat{T} + R_m + \zeta_j + \epsilon^{(j)} \tag{16}$$

$$\phi^{(j)}_{\text{IF,GPS}} = \| \overrightarrow{x}^{(j)}_s - \overrightarrow{x}_{rx} + \Delta\overrightarrow{\gamma}_j \| + \left(b_{\text{GPS}} - b^{(j)}_s \right) + m^{(j)} \nabla \hat{T} + A^{(j)} + R_m + \zeta_j + \epsilon^{(j)} \tag{17}$$

$$\phi^{(j)}_{\text{IF,GAL}} = \| \overrightarrow{x}^{(j)}_s - \overrightarrow{x}_{rx} + \Delta\overrightarrow{\gamma}_j \| + \left(b_{\text{GPS}} + \Delta\beta_{\text{GPS,GAL}} - b^{(j)}_s \right) + m^{(j)} \nabla \hat{T} + A^{(j)} + R_m + \zeta_j + \epsilon^{(j)} \tag{18}$$

$$\phi^{(j)}_{\text{IF,GAL}} = \| \overrightarrow{x}^{(j)}_s - \overrightarrow{x}_{rx} + \Delta\overrightarrow{\gamma}_j \| + \left(b_{\text{GPS}} + \Delta\beta_{\text{GPS,GAL}} - b^{(j)}_s \right) + m^{(j)} \nabla \hat{T} + A^{(j)} + R_m + \zeta_j + \epsilon^{(j)} \tag{19}$$

If j^{th} satellite is GPS signal, Eq.16 and 17 are used, and Eq.18 and 19 are used if it is Galileo signal. The only difference for Eq.16, 17 and Eq.18, 19 is the receiver dependent GPS-Galileo time offset, $\Delta\beta_{\text{GPS,GAL}}$.

We can relate the receiver clock bias of GPS and Galileo with this state:

$$b_{\text{GAL}} = b_{\text{GPS}} + \Delta\beta_{\text{GPS,GAL}} \tag{20}$$

$\Delta\beta_{\text{GPS,GAL}}$ can be considered as the combination of general GPS-Galileo Time Offset (GGTO), and the hardware delay for different signals inside the receiver. This delay is pertained to how the receivers are manufactured and the frequency of signals received. It is found that the time offset varies across the receivers and we cannot ignore the differences. As a result, we define $\Delta\beta_{\text{GPS,GAL}}$ for each receiver that receives both GPS and Galileo signals. Since $\Delta\beta_{\text{GPS,GAL}}$ is mainly the instrumental delay introduced from the receiver hardware, it is relatively stable and do not change overtime. The prior for $\Delta\beta_{\text{GPS,GAL}}$ can therefore be zero process noise, similar to ambiguity for carrier phase. $\Delta\beta_{\text{GPS,GAL}}$ enables us to utilize signals from GPS and Galileo into the centralized filter without introducing additional uncertainty to the system.

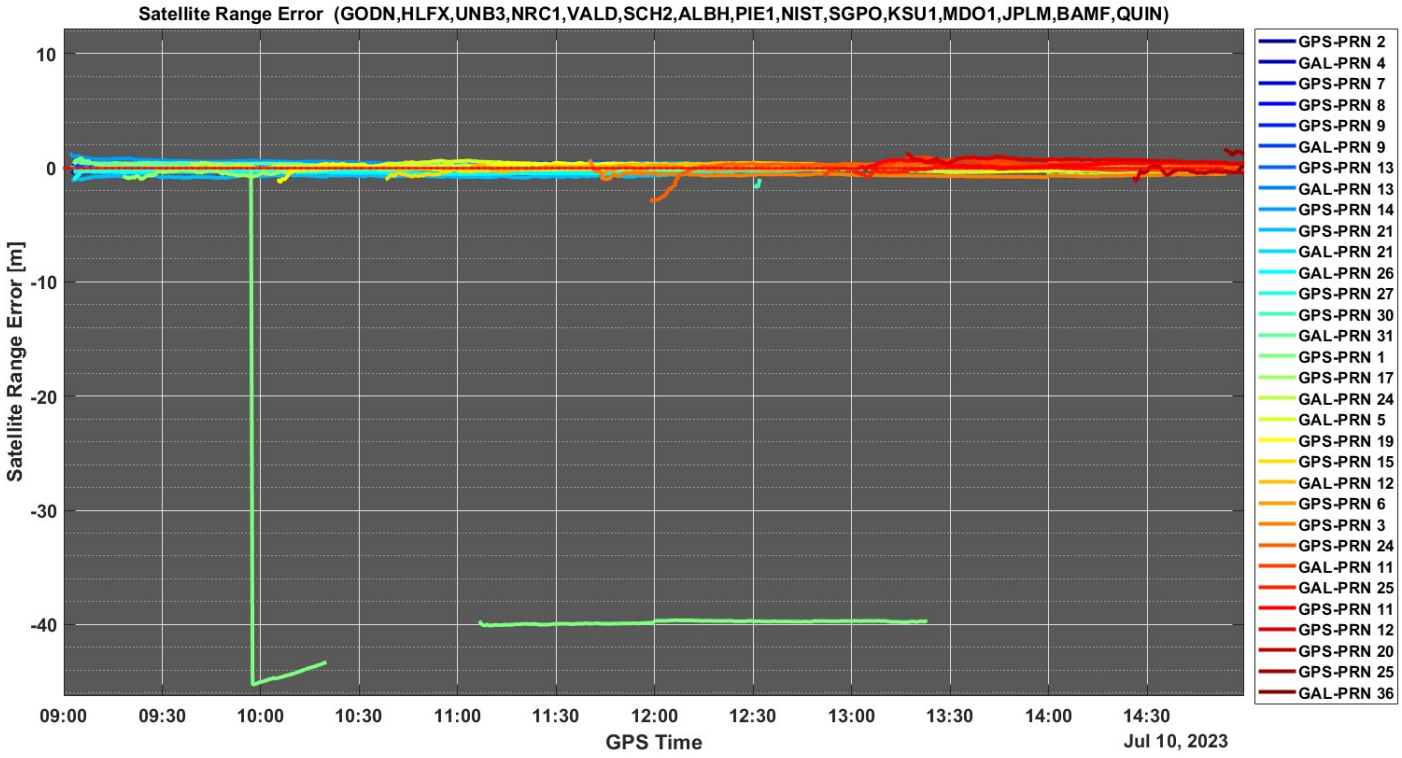

Figure 8: Single fault absolute user range error estimate.

Fig.8 is the user range errors of both GPS and Galileo satellites the 15 IGS stations monitored. There was no Galileo faults happened on July 10^{th} so only the -40 m clock fault of GPS-PRN-1 is detected when no artificial faults are injected. Since there are more satellites available to the receiver network, the monitor system can tolerate more number of satellites faulted concurrently.

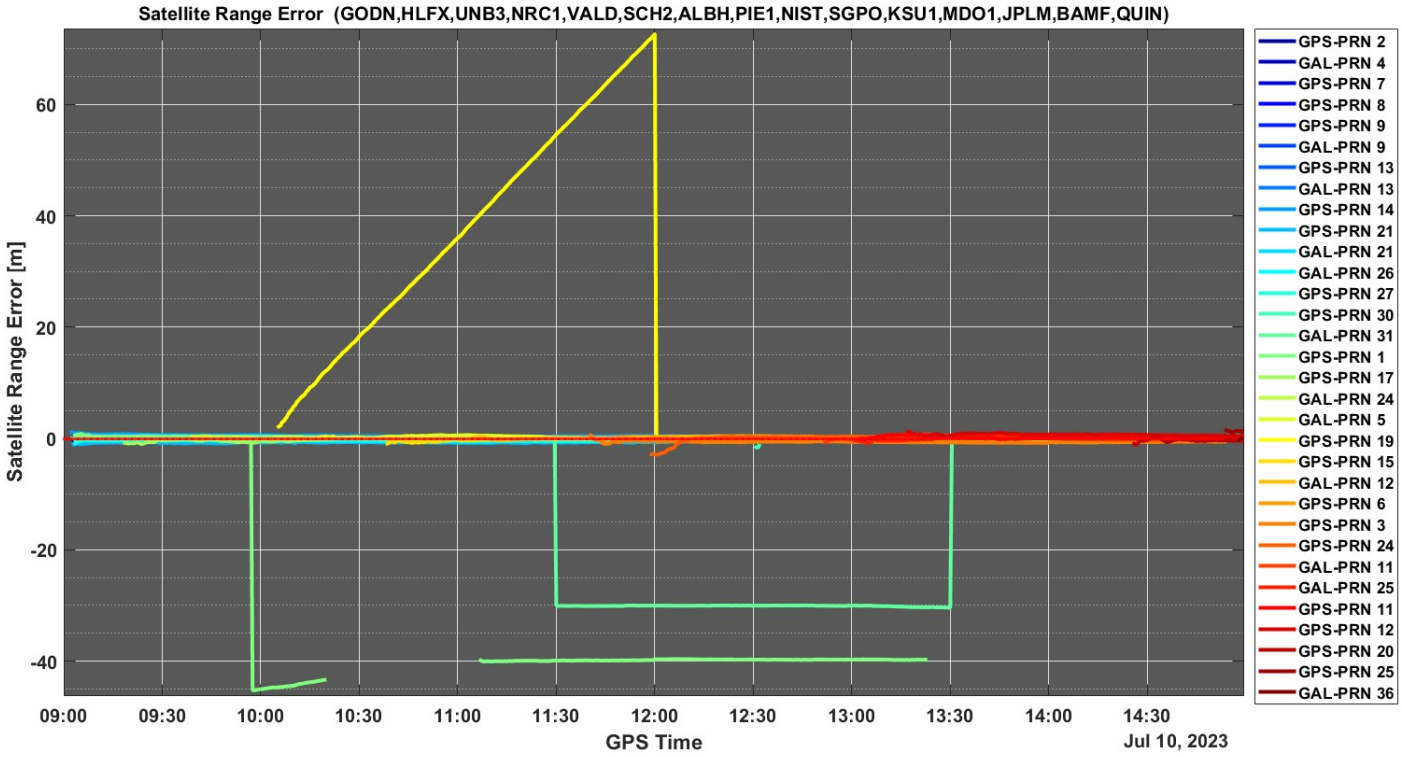

Figure 9: Multiple fault absolute user range error estimate.

Fig.9 shows the user range errors with 3 satellites clock faults happening at the same time. One is the real satellite clock fault, the -40 m step fault on GPS-PRN-1 and other two faults are artificial fault injected to GPS-PRN-19 and GAL-PRN-31. The ramp fault injected to GPS-PRN-19 is identical to the one injected in Fig.7, and the fault injected to GAL-PRN-31 is a -30 m step fault from 11:30:00∼13:30:00. There are around 16 satellites in-view to the receiver network at a time so the monitor filter can correctly identify the faulted satellites when less than 8 satellite faults occur simultaneously. The 3 satellite faults are all correctly detected in this case.

VII. CONCLUSION

The centralized filter formulated in Lai et al. (2024) is augmented to have detection states detecting all the satellites that are in-view to the receiver network. Additional constraints are applied to the filter to ensure the system is observable. The choice of the constraints is arbitrary and the zero mean constraints are chosen at the position of the receivers to have the estimate of ephemeris error and satellite clock bias error meaningful and easier to be interpreted. GNSS code phase and carrier phase measurements from IGS are used to evaluate the performance of the all-in-view centralized filter. We used code phase and carrier phase data from 15 IGS receivers located across North America on July 10^{th}, 2023, when a -40 m step fault happened on GPS-PRN-1. The all-in-view centralized filter successfully detects the step fault. We then injected 1 artificial faults to GPS-PRN-19 along with the original step fault on PRN-1. The all-in-view centralized filter also detects and separates the 2 faulted satellites from the normal satellites. We rely on the fact that the majority of the satellites behave nominally, so we can identify which satellites are at fault from the range error estimates by leveraging the likelihood of the normal and faulted satellites. We can compute for the bias of the user range error estimate such that the likelihood of the user range error is maximized after applying the offset to the user range error estimates. The bias also provides the absolute user range error estimates instead of the relative user range error from the estimation. This strategy would inevitably fail if more than half of the satellites in-view to the receivers are faulted, which can be improved by including more constellation to the centralized filter. Finally, we include signals from Galileo constellation to the centralized filter and inject another artificial fault to GAL-PRN-31, along with the artificial fault on GPS-PRN-19 and real clock fault on GPS-PRN-1. It is shown that the filter successfully detected all 3 faults happened at the same time, and obtain the correct absolute user range error. We showed that the all-in-view centralized filter can detect multiple faults happened simultaneously and estimate the absolute user range error at any user location without applying solution separation on the satellite exclusions.

ACKNOWLEDGEMENTS

We gratefully acknowledge the support of the Hexagon and NovAtel Inc. for funding this work. We also thank the FAA Satellite Navigation Team for funding this work under Memorandum of Agreement #: 693KA8-22-N-00015.

REFERENCES

Blanch, J., Ouk, S., Pullen, S., Lo, S., and Walter, T. (2024). Advanced raim for mega-constellations. In *Proceedings of the 37th International Technical Meeting of the Satellite Division of The Institute of Navigation (ION GNSS+ 2024)*, pages –.

Blanch, J., Walker, T., Enge, P., Lee, Y., Pervan, B., Rippl, M., Spletter, A., and Kropp, V. (2015). Baseline advanced raim user algorithm and possible improvements. *IEEE Transactions on Aerospace and Electronic Systems*, 51(1):713–732.

Gunning, K., Blanch, J., Walter, T., de Groot, L., and Norman, L. (2018). Design and evaluation of integrity algorithms for ppp in kinematic applications. In *Proceedings of the 31st International Technical Meeting of the Satellite Division of The Institute of Navigation (ION GNSS+ 2018)*, pages 1910–1939.

IGS, M. (2024). International gnss service.

Lai, Y.-F., Blanch, J., and Walter, T. (2024). Ppp range error integrity using a network of ground monitors. In *Proceedings of the 37th International Technical Meeting of the Satellite Division of The Institute of Navigation (ION GNSS+ 2024)*, pages –.